$MEND_{SUV}$ can efficiently suppress endogenous gene expression and consequently enhance dendritic cell-based vaccine potency *in vivo*.

4. Discussion

In the present study, we report on the successful development of an efficient siRNA carrier (R8/GALA-$MEND_{SUV}$) which is applicable to manipulating the function of BMDCs. In this improvement process, quantitative information concerning the intracellular trafficking of siRNA was used to clarify the drawbacks of the carriers that needed to be overcome. It has been reported that siRNA is rapidly degraded in the cytosol [29]. Therefore, the efficiencies of endosomal escape and dissociation were quantified at an earlier time post-transfection (2.5 h and 9 h, respectively) to minimize the effect of siRNA degradation, while gene knockdown activity was evaluated at 48-h post-transfection.

Concerning endosomal escape, we recently demonstrated that R8-modified liposomes composed of DOPE/PA = 7/2 are capable of enhancing the cytoplasmic delivery of encapsulated molecules derived from its high fusogenic activity to endosomes [28]. Since the replacement of R8 with octa-lysine (K8) diminished the gene knockdown activity of siRNA due to a decrease in membrane-fusion efficiency at acidic pH used, R8 and the lipid composition may synergistically function in membrane fusion. Moreover, we also demonstrated that the surface modification of GALA, a pH-sensitive fusogenic peptide permits an enhanced endosomal escape in response to the low pH in endosomes [19,23,24]. In spite of these combinatorial devices, the only a slight gene knockdown effect (Fig. 1d; blue bar) was observed even in R8/GALA-$MEND_{hydo}$ with a high (approx. 70%) endosomal escape efficiency (Fig. 2). This indicates that an improvement in endosomal escape is not sufficient for effective siRNA delivery.

Since endosomal escape is coupled with a membrane fusion, it is expected that particles are released to the cytosol as a dissociated form. However, as observed in MENDs encapsulating pDNA, electron microscopic observations showed that the MENDs prepared with lipid hydration has a multi-lamellar membrane structure [27]. Therefore, we hypothesized that siRNA was released into the cytosol while still associated with excess amount of lipid envelope, and thus fails in effective gene knockdown. Importance of dissociation processes in the effective function of cargo was also shown in a pDNA-loading MEND. It was recently demonstrated that the incorporation of short PEG-modified lipids (i.e. tetraethyleneglycol (TEG)-conjugated cholesterol) is useful in controlling the number of lipid envelopes, resulting in an improvement in particle uniformity with a reduced particle size. The TEG-modified lipid particles can enhance not only cellular uptake, but also transcription activity by improving intracellular decoating, resulting in an improvement in transfection activity of more than 100-fold [30]. Although the structure of the R8/GALA-$MEND_{SUV}$ prepared with siRNA core remains to be clarified, we hypothesize that the negatively charged SUVs may be assembled around the positively charged core, and then triggers the encapsulation of the core complex through membrane fusion with neighboring SUVs to confer the coating with the di-lamellar endosome-fusogenic lipid envelope (Supplemental Fig. 2). The particle formation of di-lamellar envelope structure by incubation with pDNA core and liposomes has also been proposed previously [31]. Then, similar to this TEG-modified pDNA particle, coating with a limited amount of endosome-fusogenic lipid envelope may facilitate the intracellular decoating of the siRNA particle, triggered by the membrane fusion of the envelope with endosomes. While cellular uptake was slightly improved in the case of the R8/GALA-$MEND_{SUV}$ compared with the R8/GALA-$MEND_{hydo}$, the extent (at a maximum 2 fold) is not sufficient to explain the effective gene knockdown at 1/10 of the dose. The efficient dissociation of siRNA in the R8/GALA-$MEND_{SUV}$ in comparison with R8/GALA-$MEND_{hydo}$ (Fig. 3) is a key process for improving gene knockdown efficiency. It is plausible, however, that the surface modification of an endosome-fusogenic peptide (GALA) on a limited number of envelopes is advantageous for the dissociation of siRNA from the carriers, this would be coincident with endosomal escape.

As antigen presenting cells, DCs play a crucial role in the initiation of an immune response and the regulation of cell-mediated immune reactions. Genetic modification of DCs has been demonstrated to be effective for cancer immunotherapy. One of the strategies for achieving this is to enhance the life-span of DCs by the introduction of antiapoptotic genes (Bcl-X_L and Bcl-X_{FNK}) genes [32] or the gene knockdown of apoptotic genes (Bak and Bax) [33]. Extension of the life-span is correlated with enhanced vaccine efficiency. Another strategy would be to knockdown immunosuppressive proteins [7,8]. As a demonstration of the potential utility of R8/GALA-$MEND_{SUV}$ in *in vivo* use, siRNA targeting SOCS1, was introduced to the BMDCs and enhanced immunoresponse against cancer (Fig. 4). BMDCs transfected with anti-SOCS1 showed more effective tumor growth inhibition compared with those treated with control siRNA. However, even in the SOCS1-knockdown group, significant tumor growth starts to appear at 20 days after tumor inoculation. While the mechanism for the loss of function has not been clarified, one of the most plausible reasons is the short half-life of the DCs. A combination of SOCS1 gene knockdown and extending the half-life of DCs by the introduction of antiapoptotic genes [32] or the gene knockdown of apoptotic genes [33] may lead to a more potent and more long-lasting tumor vaccination system.

Currently many experiments are being conducted with cationic liposome-based transfection reagents including LFN2000. However, the introduction of nucleic acids such as plasmid DNA and siRNA into *ex vivo* cultured DCs appears to be difficult. In addition, some cationic lipids have immunostimulating activity which might cause undesirable side effects. Yan et al. showed that a cationic lipid (i.e. DOTAP), stimulates BMDCs through the generation of reactive oxygen species (ROS) and induces chemokine, cytokine and co-stimulatory molecules (CD86/CD80) [34]. The DOTAP liposome showed *in vivo* antitumor effects by lipid itself at an optimal dose. On the other hand, high levels of DOTAP-generated ROS cause apoptosis in dendritic cells. Therefore, an effective and substantially non-stimulating delivery system would be highly desirable. In a previous study, Nakamura et al. reported that R8-modified liposomes did not show non-specific antitumor effects *in vivo* [35]. Therefore, the R8/GALA-MEND system was expected to have minor immunostimulatory effects. We recently demonstrated that the encapsulation of OVA in R8-modified liposomes drastically inhibits E.G.7-OVA tumor growth after subcutaneous immunization, compared with that for an OVA solution [35]. A combination of antigen delivery and regulation of the signaling pathway by siRNA delivery with R8-modified particles may prove to be an innovative cancer vaccine.

In summary, a quantitative evaluation of intracellular trafficking revealed that dissociation, as well as the endosome escape process is significant rate-limiting processes for siRNA. GALA modification and reducing the number of lipid envelopes contribute to the successful improvement of the siRNA carrier, which can be applied to BMDC for *ex vivo* cancer vaccine.

Acknowledgements

This work was supported by CREST from the Japan Science and Technology Agency (JST), Grant for Industrial Technology Research from the New Energy and Industrial Technology Development Organization (NEDO) and in part by the Japan Society for the Promotion of Science. The authors thank Dr. Milton S. Feather for his helpful advice in writing the English manuscript.

Appendix A. Supplementary data

Supplementary data associated with this article can be found, in the online version, at doi:10.1016/j.jconrel.2010.01.012.

References

[1] S.M. Elbashir, J. Harborth, W. Lendeckel, A. Yalcin, K. Weber, T. Tuschl, Duplexes of 21-nucleotide RNAs mediate RNA interference in cultured mammalian cells, Nature 411 (6836) (2001) 494–498.

[2] A. Fire, S. Xu, M.K. Montgomery, S.A. Kostas, S.E. Driver, C.C. Mello, Potent and specific genetic interference by double-stranded RNA in *Caenorhabditis elegans*, Nature 391 (6669) (1998) 806–811.

[3] S. Akhtar, I.F. Benter, Nonviral delivery of synthetic siRNAs in vivo, J. Clin. Invest. 117 (12) (2007) 3623–3632.

[4] D. Grimm, M.A. Kay, Therapeutic application of RNAi: is mRNA targeting finally ready for prime time? J. Clin. Invest. 117 (12) (2007) 3633–3641.

[5] D. Haussecker, The business of RNAi therapeutics, Hum. Gene Ther. 19 (5) (2008) 451–462.

[6] T. Naka, M. Narazaki, M. Hirata, T. Matsumoto, S. Minamoto, A. Aono, N. Nishimoto, T. Kajita, T. Taga, K. Yoshizaki, S. Akira, T. Kishimoto, Structure and function of a new STAT-induced STAT inhibitor, Nature 387 (6636) (1997) 924–929.

[7] L. Shen, K. Evel-Kabler, R. Strube, S.Y. Chen, Silencing of SOCS1 enhances antigen presentation by dendritic cells and antigen-specific anti-tumor immunity, Nat. Biotechnol. 22 (12) (2004) 1546–1553.

[8] X.T. Song, K. Evel-Kabler, L. Rollins, M. Aldrich, F. Gao, X.F. Huang, S.Y. Chen, An alternative and effective HIV vaccination approach based on inhibition of antigen presentation attenuators in dendritic cells, PLoS Med. 3 (1) (2006) e11.

[9] S.E. Raper, N. Chirmule, F.S. Lee, N.A. Wivel, A. Bagg, G.P. Gao, J.M. Wilson, M.L. Batshaw, Fatal systemic inflammatory response syndrome in a ornithine transcarbamylase deficient patient following adenoviral gene transfer, Mol. Genet. Metab. 80 (1–2) (2003) 148–158.

[10] S. Hacein-Bey-Abina, C. von Kalle, M. Schmidt, F. Le Deist, N. Wulffraat, E. McIntyre, I. Radford, J.L. Villeval, C.C. Fraser, M. Cavazzana-Calvo, A. Fischer, A serious adverse event after successful gene therapy for X-linked severe combined immunodeficiency, N. Engl. J. Med. 348 (3) (2003) 255–256.

[11] S. Zhang, B. Zhao, H. Jiang, B. Wang, B. Ma, Cationic lipids and polymers mediated vectors for delivery of siRNA, J Control Release 123 (1) (2007) 1–10.

[12] S. Chono, S.D. Li, C.C. Conwell, L. Huang, An efficient and low immunostimulatory nanoparticle formulation for systemic siRNA delivery to the tumor, J Control Release 131 (1) (2008) 64–69.

[13] S.D. Li, L. Huang, Targeted delivery of antisense oligodeoxynucleotide and small interference RNA into lung cancer cells, Mol. Pharm. 3 (5) (2006) 579–588.

[14] D.V. Morrissey, J.A. Lockridge, L. Shaw, K. Blanchard, K. Jensen, W. Breen, K. Hartsough, L. Machemer, S. Radka, V. Jadhav, N. Vaish, S. Zinnen, C. Vargeese, K. Bowman, C.S. Shaffer, L.B. Jeffs, A. Judge, I. MacLachlan, B. Polisky, Potent and persistent in vivo anti-HBV activity of chemically modified siRNAs, Nat. Biotechnol. 23 (8) (2005) 1002–1007.

[15] T.S. Zimmermann, A.C. Lee, A. Akinc, B. Bramlage, D. Bumcrot, M.N. Fedoruk, J. Harborth, J.A. Heyes, L.B. Jeffs, M. John, A.D. Judge, K. Lam, K. McClintock, L.V. Nechev, L.R. Palmer, T. Racie, I. Rohl, S. Seiffert, S. Shanmugam, V. Sood, J. Soutschek, I. Toudjarska, A.J. Wheat, E. Yaworski, W. Zedalis, V. Koteliansky, M. Manoharan, H.P. Vornlocher, I. MacLachlan, RNAi-mediated gene silencing in non-human primates, Nature 441 (7089) (2006) 111–114.

[16] K. Kogure, H. Akita, H. Harashima, Multifunctional envelope-type nano device for non-viral gene delivery: concept and application of Programmed Packaging, J. Control. Release 122 (3) (2007) 246–251.

[17] K. Kogure, H. Akita, Y. Yamada, H. Harashima, Multifunctional envelope-type nano device (MEND) as a non-viral gene delivery system, Adv. Drug Deliv. Rev. 60 (4–5) (2008) 559–571.

[18] Y. Nakamura, K. Kogure, S. Futaki, H. Harashima, Octaarginine-modified multifunctional envelope-type nano device for siRNA, J. Control. Release 119 (3) (2007) 360–367.

[19] T. Kakudo, S. Chaki, S. Futaki, I. Nakase, K. Akaji, T. Kawakami, K. Maruyama, H. Kamiya, H. Harashima, Transferrin-modified liposomes equipped with a pH-sensitive fusogenic peptide: an artificial viral-like delivery system, Biochemistry 43 (19) (2004) 5618–5628.

[20] H. Akita, R. Ito, I.A. Khalil, S. Futaki, H. Harashima, Quantitative three-dimensional analysis of the intracellular trafficking of plasmid DNA transfected by a nonviral gene delivery system using confocal laser scanning microscopy, Mol. Ther. 9 (3) (2004) 443–451.

[21] S. Hama, H. Akita, R. Ito, H. Mizuguchi, T. Hayakawa, H. Harashima, Quantitative comparison of intracellular trafficking and nuclear transcription between adenoviral and lipoplex systems, Mol. Ther. 13 (4) (2006) 786–794.

[22] T. Akazawa, H. Masuda, Y. Saeki, M. Matsumoto, K. Takeda, K. Tsujimura, K. Kuzushima, T. Takahashi, I. Azuma, S. Akira, K. Toyoshima, T. Seya, Adjuvant-mediated tumor regression and tumor-specific cytotoxic response are impaired in MyD88-deficient mice, Cancer Res. 64 (2) (2004) 757–764.

[23] W. Li, F. Nicol, F.C. Szoka Jr., GALA: a designed synthetic pH-responsive amphipathic peptide with applications in drug and gene delivery, Adv. Drug Deliv. Rev. 56 (7) (2004) 967–985.

[24] S. Nir, F. Nicol, F.C. Szoka Jr., Surface aggregation and membrane penetration by peptides: relation to pore formation and fusion, Mol. Membr. Biol. 16 (1) (1999) 95–101.

[25] R.A. Parente, S. Nir, F.C. Szoka Jr., pH-dependent fusion of phosphatidylcholine small vesicles. Induction by a synthetic amphipathic peptide, J. Biol. Chem. 263 (10) (1988) 4724–4730.

[26] K. Sasaki, K. Kogure, S. Chaki, Y. Nakamura, R. Moriguchi, H. Hamada, R. Danev, K. Nagayama, S. Futaki, H. Harashima, An artificial virus-like nano carrier system: enhanced endosomal escape of nanoparticles via synergistic action of pH-sensitive fusogenic peptide derivatives, Anal. Bioanal. Chem. (2008).

[27] H. Akita, A. Kudo, A. Minoura, M. Yamaguti, I.A. Khalil, R. Moriguchi, T. Masuda, R. Danev, K. Nagayama, K. Kogure, H. Harashima, Multi-layered nanoparticles for penetrating the endosome and nuclear membrane via a step-wise membrane fusion process, Biomaterials 30 (15) (2009) 2940–2949.

[28] A. El-Sayed, I.A. Khalil, K. Kogure, S. Futaki, H. Harashima, Octaarginine- and octalysine-modified nanoparticles have different modes of endosomal escape, J. Biol. Chem. 283 (34) (2008) 23450–23461.

[29] Y.L. Chiu, T.M. Rana, siRNA function in RNAi: a chemical modification analysis, Rna 9 (9) (2003) 1034–1048.

[30] T. Masuda, H. Akita, K. Niikura, T. Nishio, M. Ukawa, K. Enoto, R. Danev, K. Nagayama, K. Ijiro, H. Harashima, Envelope-type lipid nanoparticles incorporating a short PEG-lipid conjugate for improved control of intracellular trafficking and transgene transcription, Biomaterials 30 (27) (2009) 4806–4814.

[31] R.J. Lee, L. Huang, Folate-targeted, anionic liposome-entrapped polylysine-condensed DNA for tumor cell-specific gene transfer, J. Biol. Chem. 271 (14) (1996) 8481–8487.

[32] T. Yoshikawa, T. Niwa, H. Mizuguchi, N. Okada, S. Nakagawa, Engineering of highly immunogenic long-lived DC vaccines by antiapoptotic protein gene transfer to enhance cancer vaccine potency, Gene Ther. 15 (19) (2008) 1321–1329.

[33] T.W. Kim, J.H. Lee, L. He, D.A. Boyd, J.M. Hardwick, C.F. Hung, T.C. Wu, Modification of professional antigen-presenting cells with small interfering RNA in vivo to enhance cancer vaccine potency, Cancer Res 65 (1) (2005) 309–316.

[34] W. Yan, W. Chen, L. Huang, Reactive oxygen species play a central role in the activity of cationic liposome based cancer vaccine, J. Control. Release 130 (1) (2008) 22–28.

[35] T. Nakamura, R. Moriguchi, K. Kogure, N. Shastri, H. Harashima, Efficient MHC class I presentation by controlled intracellular trafficking of antigens in octaarginine-modified liposomes, Mol. Ther. 16 (8) (2008) 1507–1514.

Enhanced Target-Specific Accumulation of Radiolabeled Antibodies by Conjugating Arginine-Rich Peptides as Anchoring Molecules

Rei Miyamoto,[†] Hiromichi Akizawa,[‡] Takeshi Nishikawa,[†] Tomoya Uehara,[†] Yusuke Azuma,[§] Ikuhiko Nakase,[§] Shiroh Futaki,[§] Hirofumi Hanaoka,[∥] Yasuhiko Iida,[⊥] Keigo Endo,[∥] and Yasushi Arano*[,†]

Graduate School of Pharmaceutical Sciences, Chiba University, 1-8-1 Inohana, Chuo-ku, Chiba 260-8675, Japan, Graduate School of Pharmaceutical Sciences, Health Sciences University of Hokkaido, 1757 Kanazawa, Tobetsu-cho, Ishikari-gun, Hokkaido 061-0293, Japan, Institute for Chemical Research, Kyoto University, Gokasho, Uji, Kyoto 611-0011, Japan, Graduate School of Medicine, Gunma University, 39-22, Showa-machi 3-chome, Maebashi, Gunma 371-8511, Japan, and Suzuka University of Medical Science, 1001-1 Kishioka-cho, Suzuka, Mie 510-0293, Japan. Received June 8, 2010; Revised Manuscript Received August 23, 2010

We have devised and estimated a new strategy to prolong the residence time of radiolabeled antibodies in tumor in which an octaarginine peptide (R_8) was used as an anchoring molecule to fix antibodies against CD20 (NuB2; IgG2a) on tumor cells. Conjugation of R_8 with antibodies was performed by maleimide−thiol chemistry using thiol groups generated by reducing the disulfide bonds of the antibody. The R_8-conjugated NuB2 was then reacted with succinimidyl *meta*-[^{125}I]iodobenzoate to prepare [^{125}I]SIB-NuB2$_I$ (0.92 R_8/NuB2) and [^{125}I]SIB-NuB2$_{III}$ (3.38 R_8/NuB2). Both SIB-NuB2$_I$ and SIB-NuB2$_{III}$ exhibited size-exclusion HPLC elution profiles and immunoreactivity to CD20-positive cells similar to those of NuB2. NuB2$_I$ also possessed isoelectric focusing (IEF) profile similar to NuB2. However, NuB2$_{III}$ registered a broad IEF band toward higher pI. When incubated with CD20-positive cells, [^{125}I]SIB-NuB2$_I$ and [^{125}I]SIB-NuB2$_{III}$ exhibited 1.4 and 4.0 times higher cell-associated radioactivity than [^{125}I]SIB-NuB2. After the cells were washed and reincubated in a fresh medium for 3 h, [^{125}I]SIB-NuB2$_I$ and [^{125}I]SIB-NuB2$_{III}$ exhibited significantly higher cell-associated radioactivity than [^{125}I]SIB-NuB2. In biodistribution studies in normal mice, while both [^{125}I]SIB-NuB2$_I$ and [^{125}I]SIB-NuB2 exhibited similar biodistribution profiles, [^{125}I]SIB-NuB2$_{III}$ showed faster clearance from the blood and higher hepatic radioactivity levels than [^{125}I]SIB-NuB2. In SCID mice bearing CD20-positive xenografts, [^{131}I]SIB-NuB2$_I$ exhibited significantly higher radioactivity in xenografts than those of [^{125}I]SIB-NuB2 with no significant increase being observed in other tissues. The findings indicate that appropriate R_8 modification of antibodies satisfies both specific targeting ability of antibody and strong cell-association property of R_8, which was reflected in the increased radioactivity levels in tumor. These findings supported the applicability of this approach to enhance target-specific accumulation of radiolabeled antibodies.

INTRODUCTION

Radioimmunotherapy (RIT) is a cancer therapeutic modality that combines the specific tumor targeting of immunotherapeutics and cytotoxic radiation mechanisms. Encouraging results have been reported in patients with hematologic malignancies treated with ^{90}Y- and ^{131}I-labeled antibodies against CD20 (*1*−*4*), due to their intrinsic high radiosensitivity and relatively good access of the radiolabeled antibodies to the cancer cells (*5, 6*). Despite numerous efforts, the treatment of solid tumors with radiolabeled antibodies resulted in limited success, due to poor localization of radiolabeled antibodies in the tumors (*7*−*9*). Thus, the enhancement of tumor accumulation and retention of radiolabeled antibodies constitutes a prime requisite for successful RIT.

Numerous factors have been presented as being responsible for tumor accumulation and retention of radiolabeled antibodies (*8*). Since the mechanism of accumulation of radiolabeled antibodies is based on their specific but reversible binding to antigens in tumor tissues, a strategy that shifts the equilibrium to antigen association was considered of prime importance to enhancing tumor accumulation. The use of antibodies internalized to target cells would prolong residence time in the tumor, since these molecules will be resistant to being cleared by washout. The conjugation of arginine-rich cell-penetrating peptides (AR-CPPs) to antibodies has been conducted as a means to facilitate internalization of antibodies and to increase tumor accumulation. Indeed, a prior study reported an increase in tumor accumulation of AR-CPP-conjugated antibodies in vitro (*10*). However, in vivo studies showed increased accumulation in nontarget tissues such as the liver with decreased accumulation in tumors. A prior study also described that the tumor targeting ability of an antibody construct (scFv) was completely abolished following conjugation with AR-CPP (*11*).

Meanwhile, an increase in avidity of antibodies constitutes another strategy to enhance tumor accumulation, as observed in antibody constructs with multivalent binding domains (*8, 12, 13*). An increase in tumor uptake was also observed with divalent radiolabeled haptens in pretargeting strategy (*14*). These studies suggested that chemical modification of antibodies with anchoring molecules that possess strong interaction with cell surface molecules or cell membrane may also be useful to shift the equilibrium to antigen association in tumor tissues.

* Corresponding author. Yasushi Arano, Ph.D. Graduate School of Pharmaceutical Sciences, Chiba University, 1-8-1 Inohana, Chuo-ku, Chiba 260-8675, Japan. Phone: +81-43-226-2896; Fax: +81-43-226-2897; E-mail: arano@p.chiba-u.ac.jp.

[†] Chiba University.

[‡] Health Sciences University of Hokkaido.

[§] Kyoto University.

[∥] Gunma University.

[⊥] Suzuka University of Medical Science.

10.1021/bc100259q
Published on Web 10/25/2010

Scheme 1

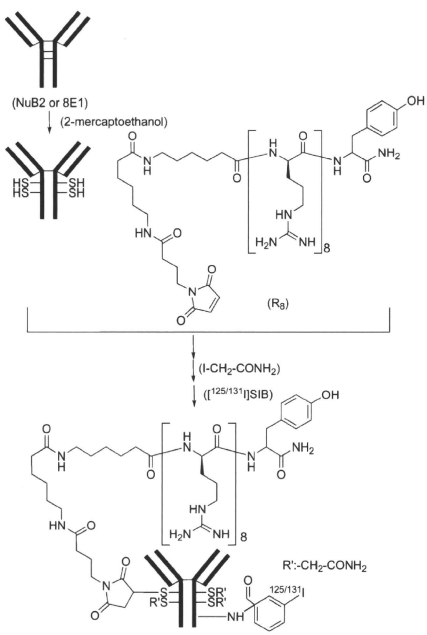

The AR-CPPs possess strong interaction with phosphate groups, sulfates, and carboxylates on cellular components (*15*−*18*). The electrostatic interaction between AR-CPPs and cell membrane is so strong that complete removal of AR-CPPs from the cell surface is difficult to perform (*19*−*21*). Such characteristics render AR-CPPs applicable as an anchoring molecule to shift the equilibrium to antigen association for prolonged retention of radiolabeled antibodies in tumors. In addition, the strong electrostatic interaction between AR-CPPs and cellular components suggested that AR-CPPs would exert their anchoring ability at conjugation levels much lower than those used for facilitating internalization.

In this study, an octaarginine peptide was selected as an anchoring molecule, and the peptide was derivatized with a maleimide group to conjugate with a relevant or irrelevant antibody against CD20 (Scheme 1). After radiolabeling of the modified antibodies with succinimidyl *meta*-[$^{125/131}$I]iodobenzoate ([$^{125/131}$I]SIB), the effect of the octaarginine conjugation on specific binding to target cells, dissociation rates from the cells, and biodistribution was determined with special emphasis being laid on the relationship between the anchoring ability of R_8 and the number of R_8 molecules attached per molecule of the antibody. The applicability of the new approach using an AR-CPP as an anchoring molecule to prolong residence time of radiolabeled antibodies in tumor will be discussed.

EXPERIMENTAL PROCEDURES

Reagents and Chemicals. Na[^{125}I]I and Na[^{131}I]I were obtained from MP Biomedicals (Irvine) and Perkin-Elmer (Yokohama, Japan), respectively. The stannyl precursor of the radioiodination reagents, *N*-succinimidyl-3-(tri-*n*-butylstannyl)-benzoate (ATE) was synthesized as reported previously (*22*). Size-exclusion high-performance liquid chromatography (SE-HPLC) was performed using a Cosmosil Diol-300 (7.5 × 600 mm, Nacalai Tesque, Kyoto, Japan) column at a flow rate of 1 mL/min with 0.1 M phosphate buffer (PB, pH 6.8) as an eluent. Each eluent was collected with a fraction collector (RediFlac, GE Healthcare Bioscience, Tokyo, Japan) at 1 min intervals. The radioactivity counts in each fraction (1 mL) were determined with an autowell γ counter (ARC-380M, Aloka, Tokyo). TLC analyses were performed with silica plates (Silica Gel 60 F_{254}, Merck, Tokyo). Isoelectric focusing (IEF) was conducted using a Tefco STC808 mini electrophoresis cell (Tefco, Tokyo) with a precast polyacrylamide gel isoelectric focusing (IEF-PAGE) mini isocratic gel (pH 3−10) (Tefco, Tokyo). Other reagents were of reagent grade and were used as received.

Cells and Antibodies. The CD20 positive human peripheral lymphocyte line RPMI 1788 cells were incubated with RPMI-1640 medium (Sigma-Aldrich Co, St. Louis, MO, USA) supplemented with 10% fetal calf serum and were used for the studies.

The monoclonal antibodies used in this study were a murine monoclonal antibody (NuB2; IgG2b) that reacts specifically with CD20 as a relevant antibody and a murine monoclonal antibody (8E1; IgG2a) specific to a neural protein as an irrelevant one, respectively, since both subclasses possess similar quaternary structures and the interchain disulfide bonds are the primary sites of chemical reduction for both antibodies (*23*). Both antibodies were kindly supplied from Immuno-Biological Laboratories Co, Ltd., (Takasaki, Japan).

Synthesis of Mal-(Acp)$_2$-(D-Arg)$_8$-(D-Tyr) (R_8). We employed D-octaarginine peptide as an AR-CPP, and the peptide with N-terminal bis-aminocaproate linker was coupled with *N*-(4-maleimidebutyryloxy)succinimide for antibody conjugation (Scheme 1).

The peptide chain of R_8 was constructed by Fmoc (9-fluorenylmethyloxycarbonyl) solid-phase peptide synthesis on a TGS-RAM resin (Shimadzu, Kyoto) using Shimadzu PSSM8 peptide synthesizer (Shimadzu, Kyoto) with its standard protocol. A 1-[bis(dimethylamino)methylene]-1*H*-benzotriazolium 3-oxide hexafluorophosphate/1-hydroxybenzotriazole/*N*,*N*-diisopropylethylamine coupling system was employed as the coupling system. As amino acid derivatives, Fmoc-Acp, Fmoc-D-Arg(Pdf), and Fmoc-D-Tyr(^{t}Bu) were used (Acp = 6-aminocaproic acid). The peptide resin was then treated with *N*-(4-maleimidobutyryloxy)succinimide (3 equiv) and *N*-methylmorpholine (3 equiv) in DMF at 37 °C for 20 min to yield a peptide resin bearing a maleimide moiety on its N-terminus. The final deprotection of the peptide resin using trifluoroacetic acid (TFA)−H_2O (95:5) at room temperature for 3 h followed by reverse-phase HPLC purification with a Cosmosil Protein-R (10 × 250 mm, Nacalai Tesque, Kyoto) at a flow rate of 1 mL/min with a gradient mobile phase starting from 14% A (H_2O containing 0.1% TFA) and 86% B (CH_3CN containing 0.1% TFA) to 44% A and 56% B in 15 min. The product was ascertained by matrix-assisted laser desorption ionization time-of-flight mass spectrometry (MALDI-TOFMS, Voyager-DE STR, Applied Biosystems, Tokyo). MALDI-TOFMS: 1822.14 [Calcd for $(M + H)^+$: 1822.16].

Preparation of R_8-Modified Antibodies. Two R_8-modified NuB2s with different R_8-conjugation levels (NuB2$_I$ and NuB2$_{III}$) were prepared by reducing the disulfide bonds of NuB2 as reported previously with some modifications (Scheme 1) (*22*). Briefly, NuB2 was concentrated in a nitrogen atmosphere to 6.0 mg/mL in well-degassed 0.1 M PB (pH 7.0) containing 2 mM EDTA. The antibody (1.0 mL) was allowed to react with 2-mercaptoethanol (2-ME, 1000 molar excess) by gently stirring at room temperature for 30 min. Excess 2-ME was then removed

by a centrifuged column procedure using Sephadex G-50 Fine (GE Healthcare, Tokyo) equilibrated and eluted with 0.1 M PB (pH 6.0) containing 2 mM EDTA. A small aliquot of the filtrate was sampled, and the number of exposed thiol groups was determined with 2,2-dipyridyl disulfide (*24*). The filtrate was then added to a reaction vial containing 1.5-fold R_8 (42.8 μL, 85.7 μg) for $NuB2_I$ or 5-fold R_8 for $NuB2_{III}$ in 0.1 M PB (pH 6.0). After the reaction mixture was agitated gently for 1.5 h at 25 °C, 500-fold molar excess of iodoacetamide (269 μL, 2.68 mg) in 0.1 M PB (pH 6.0) was added. The reaction mixture was further incubated for 30 min to alkylate the unreacted thiol groups. $NuB2_I$ and $NuB2_{III}$ were finally purified by the centrifuged column procedure, equilibrated, and eluted with PBS (0.01 M, pH 7.4; Wako, Tokyo). Both $8E1_I$ and $8E1_{III}$ were prepared according to the procedure described above except for using 8E1 in place of NuB2.

Preparation of [$^{125/131}$I] *N*-Succinimidyl 3-Iodobenzoate (SIB)-Labeled Antibodies. *N*-Succinimidyl 3-(tri-*n*-butylstannyl)benzoate (ATE) was synthesized and radio-iodinated in the presence of *N*-chlorosuccinimide (NCS) as described previously (*25*). Briefly, ATE was dissolved in methanol containing 1% acetic acid (0.45 mg/mL), and 16.2 μL of this solution was mixed with 4.4 μL of NCS in methanol (0.5 mg/mL) in a sealed vial, followed by addition of Na[^{125}I]I (2 μL). After incubation at room temperature for 45 min, the reaction was quenched with aqueous sodium bisulfite (2.2 μL, 0.72 mg/mL). The radiochemical yield of [^{125}I]SIB was determined by TLC developed with ethyl acetate. The solvent was removed under a stream of N_2 prior to subsequent conjugation reaction with the antibodies. Conjugation of [^{125}I]SIB with antibodies was performed according to our previous procedure (*22*), with slight modifications as follows: A solution of $NuB2_I$, $NuB2_{III}$, $8E1_I$, or $8E1_{III}$ (120 μL, 2.5 mg/mL) in 0.2 M borate buffer (pH 8.5) was added to the dried residue of crude [^{125}I]SIB. After gentle incubation for 1 h at room temperature, [^{125}I]SIB-labeled antibodies were purified by the centrifuged column procedure, equilibrated, and eluted with PBS. Radioiodination of ATE with Na[^{131}I]I was performed as described above except for using Na[^{125}I]I in place of Na[^{131}I]I. Radiochemical purities of radiolabeled antibodies were also determined by SE-HPLC and TLC developed with 80% methanol/H_2O.

Preparation of ^{125}I-NuB2. Direct radioiodination of NuB2 was performed by the chloramine T method (*22*). To a solution of NuB2 (0.25 mg/mL; 200 μL) in 0.3 M PB (pH 7.5) was added 5 μL of Na[^{125}I]I. Chloramine T (0.1 mg/mL, 25 μL), freshly prepared in the same buffer, was then added. After incubation of the mixture for 10 min at room temperature, the reaction was terminated by an addition of 6 μL of aqueous sodium bisulfite (0.7 mg/mL). ^{125}I-NuB2 was purified by the centrifuged column procedure. The radiochemical purity was determined by SE-HPLC and TLC developed with 80% methanol/H_2O.

Preparation of Fluoresced Antibodies. NuB2, $NuB2_I$, and $NuB2_{III}$ were also labeled with Alexa Fluor 488 (AF, Molecular Probes, Tokyo). The fluorophore was dissolved in dimethylformamide at a concentration of 10 mg/mL, and the conjugation reaction was performed with a 5-fold molar excess of the fluorophore in 0.1 M sodium carbonate−sodium bicarbonate buffer (pH 9.0). After 1 h at room temperature, the reaction was terminated by an addition of freshly prepared 1.5 M hydroxylamine, and the fluorescent antibodies were purified by the centrifuged column procedure. The protein concentration in the purified conjugates was determined spectrophotometrically by subtracting 0.11 $A_{495\ nm}$ of the fluorophore from the $A_{280\ nm}$ of the antibody. The degree of labeling was calculated by dividing the $A_{495\ nm}$ of the fluorophore by the molar concentration of the antibodies and the dye extinction coefficient of 71 000 $M^{-1}\ cm^{-1}$.

Immunoreactivity. The immunoreactivity of radiolabeled NuB2s was assessed by the competitive immunoassay (*26*). To minimize nonspecific binding of radioiodinated antibodies to plastic tubes, the tubes were presaturated with a freshly prepared solution of 1% bovine serum albumin in PBS for 30 min, followed by three washes with PBS (*27*). Nonradioactive SIB-NuB2, $SIB\text{-}NuB2_I$, and $SIB\text{-}NuB2_{III}$ were prepared by experimental procedures similar to those used for [^{125}I]SIB-labeled antibodies, except that nonradioactive NaI was used in place of Na[^{125}I]I. A mixed solution of 50 μL ^{125}I-NuB2 and 50 μL nonradioactive SIB-NuB2, $SIB\text{-}NuB2_I$ or $SIB\text{-}NuB2_{III}$ (0.05−10 μg) was incubated in the presence of 1×10^6 RPMI 1788 cells suspended in 100 μL of PBS at 37 °C for 1 h. After centrifugation at 10 000 × *g* for 5 min, supernatant was discarded and the cell-associated radioactivity was determined using an auto γ counter.

RPMI 1788 Cell Binding and Retention. The cell binding of [^{125}I]SIB-labeled antibodies was also evaluated according to the procedure of Foulon et al. with slight modification (*28*). Approximately 1 μg each of [^{125}I]SIB-labeled antibodies was incubated with 1×10^6 RPMI 1788 cells for 1 h at 37 °C. Aliquots of cells in triplicate were removed, centrifuged, and washed with cold media. Then, the cell-associated radioactivity was determined as described above. Similar studies were conducted in the presence of 1000-fold excess of unlabeled NuB2.

The rest of the cells were resuspended in RPMI 1640 media containing 10% fetal bovine serum and 20 mM HEPES to a density of 3×10^6 cells/mL. After incubation for 1 and 3 h, aliquots of cells in triplicate were removed, centrifuged, and washed twice with cold media, and the cell-associated radioactivity was determined.

Confocal Microscopy. For each assay, 6×10^6 cells were plated into 35 mm glass-bottomed dishes. The cells were then incubated at 37 °C for 1 h with a fresh solution of NuB2, $NuB2_I$, or $NuB2_{III}$ (60 μL, 0.1 mg/mL) in cold RPMI 1640 media containing 10% FCS and 20 mM HEPES. The cells were washed twice with the same medium at 4 °C. The acidotropic dye LysoTracker Red DND-99 (Molecular Probes, Eugene, OR) was diluted in DMSO. The cells were resuspended in prewarmed (37 °C) medium containing 50 nM LysoTracker Red for 30 min. For live-cell imaging, aliquots of cells in 35 mm glass-based dishes were analyzed by confocal microscopy using a Fluoview FV500 (Olympus, Tokyo). Images were obtained at low-power laser (0.3−3.0% laser) using the 488 nm line of an argon laser. All images were obtained as 10 μm thicknesses of one planar (*xy*) section. The cells were maintained at 37 °C in a temperature-controlled box.

In Vivo Studies. Animal studies were conducted in accordance with our institutional guidelines and were approved by Chiba University Animal Care Committee. Biodistribution studies were performed by intravenous administration of a PBS solution of [^{125}I]SIB-NuB2, [^{125}I]$SIB\text{-}NuB2_I$, or [^{125}I]$SIB\text{-}NuB2_{III}$ to 6-week-old male ddY mice (Japan SLC Inc., Shizuoka, Japan). Groups of five mice, each receiving 0.3 μCi (20 μg/100 μL) of the antibodies, were used for the experiments. Organs of interest were removed and weighed, and the radioactivity counts were determined with an autowell γ counter at 1, 3, and 24 h postinjection.

Severe combined immunodeficiency (SCID) mice (C.B-17/IcrCrj-scid, Charles River Japan, Kanagawa, Japan) bearing xenograft of RPMI 1788 cells were also treated with a mixed solution of [^{131}I]$SIB\text{-}NuB2_I$ and [^{125}I]SIB-NuB2. The biodistribution of radioactivity after i.v. administration of the mixture

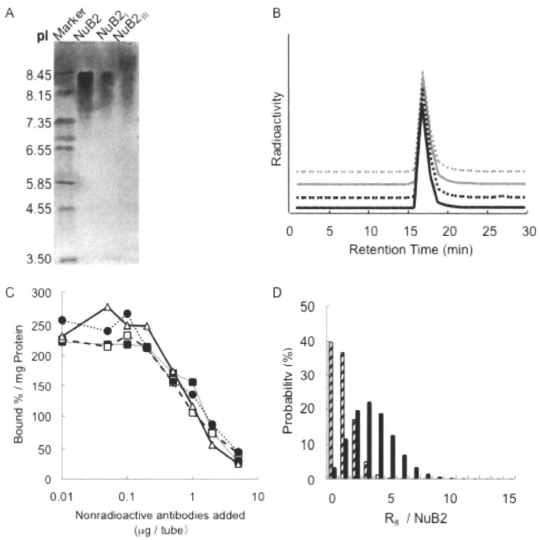

Figure 1. Characterization of R_8-conjugated antibodies ($NuB2_I$ and $NuB2_{III}$). (A) Isoelectric focusing. While both NuB2 and $NuB2_I$ showed similar profiles, a wider band toward higher pI was observed with $NuB2_{III}$. (B) Size-exclusion HPLC profiles. ^{125}I-NuB2: black solid line. [^{125}I]SIB-NuB2: black broken line. [^{125}I]SIB-$NuB2_I$: gray solid line. [^{125}I]SIB-$NuB2_{III}$: gray broken line. All the radioiodinated NuB2s exhibited similar elution profiles. (C) Competitive immunoassay to RPMI 1788 cells. Increasing concentrations of nonradioactive iodine-labeled NuB2s (NuB2 (solid square), SIB-NuB2 (square), SIB-$NuB2_I$ (circle), SIB-$NuB2_{III}$ (triangle)) and 1×10^6 RPMI 1788 cells were incubated in the presence of [^{125}I]-labeled NuB2. No significant differences were observed among the four NuB2s. (D) Poisson distribution profiles of $NuB2_I$ (hatched column) and $NuB2_{III}$ (solid column).

to 8-week-old SCID mice was monitored at 24, 48, 72, and 96 h postinjection. Groups of 5−7 mice, each receiving 0.3 μCi (10 μg each) of antibodies, were used for the experiments. Organs of interest were removed and weighed, and the radioactivity counts were determined with an autowell γ counter. A window from 29 to 97 keV was used for counting ^{125}I, whereas one from 280 to 440 keV was used for ^{131}I. Correlation factors to eliminate crossover of ^{131}I activity into ^{125}I were determined by counting ^{131}I standard in each window. The crossover of ^{125}I into the ^{131}I channel was negligible.

Statistical Analysis. Data are expressed as means ± standard deviation where appropriate. Results were statistically analyzed with an unpaired Student's *t*-test using the Microsoft *Excel* program. Differences were considered statistically significant when the *p* value was less than 0.05.

RESULTS

Preparation of Conjugates. Conjugation of NuB2 or 8E1 with R_8 was performed by maleimide−thiol chemistry using thiol groups generated by reducing the disulfide bonds of the antibody molecule. The numbers of R_8 molecule attached per molecule of NuB2 were determined to be 0.92 for $NuB2_I$ and 3.38 for $NuB2_{III}$. Similar procedures were employed for the preparation of $8E1_I$ and $8E1_{III}$ where the number of R_8 per molecule of 8E1 was estimated to be 0.98 and 3.85, respectively. The pI values of NuB2, $NuB2_I$, and $NuB2_{III}$ were determined by the isoelectric focusing and found to be 7.5−8.6, 7.5−8.6, and 7.5−9.0, respectively (Figure 1A). All [$^{125/131}$I]SIB-labeled antibodies had radiochemical purities over 95% when determined by the SE-HPLC (Figure 1B) and TLC. ^{125}I-NuB2 was prepared by the chloramine T method with radiochemical purity of 99%. AF-NuB2, AF-$NuB2_I$, and AF-$NuB2_{III}$ were labeled with Alexa Fluor 488 with a conjugation level of 3.67, 3.89, and 3.57 molecules of the fluorophore per molecule of each antibody.

Immunoreactivity Measurement. Figure 1C shows the RPMI 1788 cell binding of ^{125}I-NuB2 in the presence of unlabeled NuB2, nonradioactive SIB-conjugated NuB2, SIB-$NuB2_I$, and SIB-$NuB2_{III}$. Unlabeled NuB2 almost completely inhibited the binding of ^{125}I-NuB2 to RPMI 1788 cells, and no significant differences were observed in the inhibitory curves among the nonradioactive SIB-NuB2, SIB-$NuB2_I$, and SIB-$NuB2_{III}$. Similar results were observed with AF-labeled antibodies (data not shown).

Localization of the Antibodies in RPMI 1788 Cells. Figure 2A shows the localization of NuB2, $NuB2_I$, and $NuB2_{III}$ in living cells when determined by confocal microscopy. All AF-labeled antibodies (green) were present on the cell membrane. Under the conditions, LysoTracker (red) was observed in acidic compartment of the cells such as endosome and lysosome.

In Vitro Cell Binding and Retention. When the radiolabeled antibodies were incubated with the RPMI 1788 cell at 1 h at 37 °C, [^{125}I]SIB-$NuB2_I$ and [^{125}I]SIB-$NuB2_{III}$ showed 1.4 and 4.3 times higher cell-associated radioactivity than [^{125}I]SIB-NuB2 (Figure 2B). When the radiolabeled antibodies were incubated in the presence of 1000-fold excess of NuB2, significant reduction in the cell-associated radioactivity was observed with [^{125}I]SIB-NuB2 and [^{125}I]SIB-$NuB2_I$. However, [^{125}I]SIB-$NuB2_{III}$ still registered high cell-associated radioactivity. Similarly, higher cell-associated radioactivity was observed

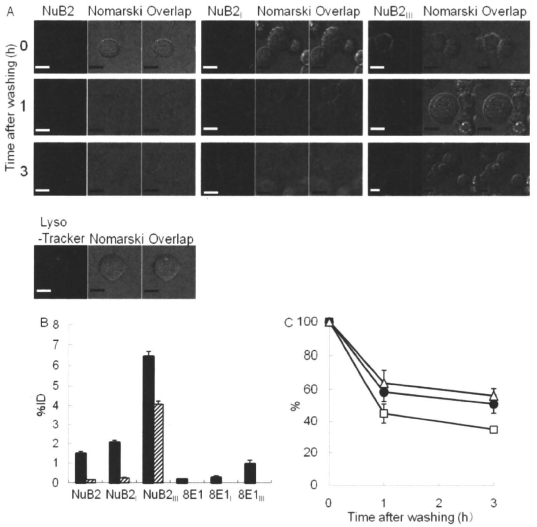

Figure 2. Cellular processing of [^{125}I]SIB-NuB2s. (A) Confocal microscopy to detect NuB2s localization (green) in RPMI 1788 cells as a function of incubation intervals at 37 °C; bars, 10 μm. (B) RPMI 1788 cell-associated radioactivity after 1 h incubation of [^{125}I]SIB-NuB2s at 37 °C (solid column). Similar experiments were performed in the presence of 1000-fold excess of NuB2 (hatched column). (C) Retention of [^{125}I]SIB-labeled NuB2s ([^{125}I]SIB-NuB2 (square), [^{125}I]SIB-NuB2$_I$ (solid circle), [^{125}I]SIB-NuB2$_{III}$ (triangle)) on RPMI 1788 cells after washing and reincubation in a fresh medium for 1 and 3 h (average of triplicates and SD).

in [^{125}I]SIB-8E1$_{III}$ when compared with [^{125}I]SIB-8E1 and [^{125}I]SIB-8E1$_I$.

Figure 2C shows the retention of [^{125}I]SIB-NuB2, [^{125}I]SIB-Nub2$_I$, and [^{125}I]SIB-NuB2$_{III}$ from RPMI 1788 cells as a function of reincubation times. While [^{125}I]SIB-NuB2 showed 44.3% and 34.2% of the initial radioactivity levels at 1 and 3 h postincubation, [^{125}I]SIB-NuB2$_I$ exhibited the cell-bound radioactivity of 59.1% and 51.2% at the same postincubation times. [^{125}I]SIB-NuB2$_{III}$ showed radioactivity levels of 67.8% and 61.3% at 1 and 3 h postincubation, respectively.

In Vivo Studies. The biodistribution of radioactivity after intravenous injection of [^{125}I]SIB-NuB2, [^{125}I]SIB-NuB2$_I$, and [^{125}I]SIB-NuB2$_{III}$ to normal mice is summarized in Table 1. Both [^{125}I]SIB-NuB2 and [^{125}I]SIB-NuB2$_I$ showed similar radioactivity levels in the blood, liver, kidney, and intestine. However, [^{125}I]SIB-NuB2$_{III}$ exhibited faster clearance of the radioactivity from the blood with higher radioactivity levels in the liver throughout the postinjection time examined. As a result, [^{125}I]SIB-NuB2$_{III}$ exhibited higher liver-to-blood ratios of the radioactivity.

Table 2 shows the biodistribution of the radioactivity after simultaneous injection of [^{125}I]SIB-NuB2 and [^{131}I]SIB-NuB2$_I$ in SCID mice bearing RPMI 1788 cells. [^{131}I]SIB-NuB2$_I$ exhibited significantly higher radioactivity levels in the tumor than those observed with [^{125}I]SIB-NuB2 from 48 to 96 h postinjection. [^{131}I]SIB-NuB2$_I$ exhibited similar radioactivity levels in other tissues such as the blood, liver, kidney, and intestine when compared with [^{125}I]SIB-NuB2.

Table 1. Biodistribution of Radioactivity after Intravenous Injection of [^{125}I]SIB-NuB2, [^{125}I]SIB-NuB2$_I$, and [^{125}I]SIB-NuB2$_{III}$ in Normal Mice[a]

	time after injection		
	1 h	3 h	24 h
	[^{125}I]SIB-NuB2		
blood	26.51 (0.99)	22.37 (1.33)	12.63 (0.48)
liver	7.65 (0.49)	5.99 (0.34)	3.34 (0.29)
kidney	5.92 (0.43)	5.46 (1.68)	3.31 (0.15)
stomach[b]	0.56 (0.55)	0.84 (0.08)	1.27 (0.44)
intestine	1.30 (0.07)	1.69 (0.15)	1.36 (0.33)
liver/blood	0.29 (0.03)	0.27 (0.00)	0.26 (0.01)
	[^{125}I]SIB-NuB2$_I$		
blood	26.26 (0.83)	20.70 (0.14)	10.54** (0.61)
liver	7.03 (0.3)	5.72 (0.33)	2.81 (0.40)
kidney	6.85* (0.31)	5.38 (0.50)	3.37 (0.35)
stomach[b]	0.58 (0.06)	1.01* (0.07)	1.89 (0.95)
intestine	1.15 (0.17)	1.68 (0.04)	0.95 (0.16)
liver/blood	0.27 (0.01)	0.28 (0.02)	0.27 (0.03)
	[^{125}I]SIB-NuB2$_{III}$		
blood	20.32 (3.79)	15.45** (1.36)	8.08** (0.49)
liver	17.91** (0.42)	14.71** (0.46)	5.85** (0.69)
kidney	6.50 (0.73)	5.80 (0.57)	3.42 (0.17)
stomach[b]	0.86** (0.05)	1.30* (0.25)	1.66 (0.67)
intestine	1.01 (0.08)	1.42 (0.30)	0.82 (0.17)
liver/blood	0.90** (0.14)	0.96** (0.12)	0.72** (0.05)

[a] Tissue radioactivity is expressed as percent of injected dose per gram of wet tissue. Results are expressed as means (SD) of three animals each point. [b] Expressed as percent of injected dose per tissue. Significances determined by unpaired Student's *t*-test. * $p < 0.05$ compared to [^{125}I]SIB-NuB2. ** $p < 0.01$ compared to [^{125}I]SIB-NuB2.

DISCUSSION

In this study, we estimate the ability of an octaarginine peptide, R_8, as an anchoring molecule to enhance target accumulation of radiolabeled antibodies. The spatial location of the anchoring molecules attached to an antibody was considered of importance to maintain antigen binding properties, specific binding, and biodistribution profiles of the parental

Table 2. Biodistribution of Radioactivity after Intravenous Injection of [^{125}I]SIB-NuB2 and [^{131}I]SIB-NuB2$_I$ in RPMI1788 Cell-Bearing SCID Mice[a]

	time after injection			
	24 h	48 h	72 h	96 h
	[^{125}I]SIB-NuB2			
blood	14.05 (1.02)	8.64 (1.18)	4.79 (1.22)	3.02 (0.39)
xenograft	4.54 (0.68)	5.36 (1.03)	3.95 (1.08)	4.81 (0.78)
liver	5.01 (0.82)	3.04 (0.39)	1.68 (0.27)	1.01 (0.10)
kidney	4.56 (0.67)	3.09 (0.50)	1.70 (0.35)	1.08 (0.22)
stomach[b]	0.33 (0.05)	0.20 (0.04)	0.38 (0.06)	0.09 (0.01)
intestine	1.15 (0.13)	1.05 (0.18)	0.58 (0.11)	0.36 (0.08)
xenograft/ blood	0.32 (0.06)	0.62 (0.09)	0.83 (0.03)	1.59 (0.35)
liver/blood	0.36 (0.07)	0.35 (0.01)	0.35 (0.04)	0.33 (0.04)
	[^{131}I]SIB-NuB2$_I$			
blood	14.60 (0.57)	8.17 (1.14)	4.58 (0.72)	2.78 (0.33)
xenograft	6.20* (0.92)	7.52* (1.19)	6.04* (1.21)	7.20** (1.32)
liver	4.33 (0.49)	2.42* (0.29)	1.39 (0.10)	0.80** (0.08)
kidney	4.78 (0.71)	2.95 (0.47)	1.57 (0.18)	1.03 (0.22)
stomach[b]	0.36 (0.06)	0.20 (0.04)	0.37 (0.07)	0.08 (0.01)
intestine	1.34 (0.19)	1.03 (0.18)	0.59 (0.08)	0.35 (0.09)
xenograft/ blood	0.42 (0.07)	0.92** (0.11)	1.31** (0.11)	2.59* (0.64)
liver/blood	0.30 (0.03)	0.30** (0.01)	0.30 (0.03)	0.29 (0.03)

[a] Tissue radioactivity is expressed as percent of injected dose per gram of wet tissue. Results are expressed as means (SD) of five to six animals for each point. [b] Expressed as percent injected dose. Significances determined by unpaired Student's *t*-test. * $p < 0.05$ compared to [^{125}I]SIB-NuB2. ** $p < 0.01$ compared to [^{125}I]SIB-NuB2.

antibodies. It was speculated that the attachment of anchoring molecules close to an antibody molecule may cause less interaction with cell surface molecules or cell membrane of target cells, whereas attachment of linkers that place the anchoring molecules at a distance from the antibody molecule may increase nonspecific binding. We selected a butyryl-bis(aminocaproate) linkage between a maleimide moiety and an octaarginine peptide with an expectation that the octaarginine moiety would not interact directly with a cell but interact strongly after the specific binding of antibody takes place. Since the importance of the density of AR-CPP molecules in an antibody was well-documented (*10, 11*), two R_8-conjugated antibodies holding different numbers of R_8 per molecule of the antibody were prepared (Scheme 1).

The R_8 conjugation and subsequent iodination reactions did not affect the SE-HPLC profiles of NuB2 (Figure 1B). The three SIB-labeled NuB2s possessed similar immunoreactivity to the antigen-positive tumor cells (Figure 1C). However, the heavy conjugation of R_8 to NuB2 increased the bandwidth of isoelectric focusing and raised pI of the resulting NuB2$_{III}$ (Figure 1A). The reaction of R_8 derivatives and an antibody can be better understood by considering the example of a perfectly random reaction (*29*). Poisson distribution can be used to predict how the R_8 molecules will be distributed among the individual antibody molecules. According to the calculation (Figure 1D), the majority of NuB2$_I$ contained up to 2 molecules of R_8 per molecule of NuB2. On the other hand, NuB2$_{III}$ consisted of a variety of conjugates ranging from 1 to 7 R_8 molecules per molecule of NuB2 with over 65% of NuB2$_{III}$ containing more than 3 R_8 molecules per molecule of NuB2, which accounts for the wide bandwidth of the isoelectric focusing.

The effect of R_8 conjugation levels on the target cell binding was assessed using CD20 positive cells. [^{125}I]NuB2$_{III}$ exhibited high cell-bound radioactivity levels even in the presence of a 1000-fold excess of cold NuB2. Since the cell-bound radioactivity levels of [^{125}I]SIB-8E1$_{III}$ were much lower than those of [^{125}I]SIB-NuB2$_{III}$, the majority of the cell-associated radioactivity of [^{125}I]NuB2$_{III}$ would be attributable to the specific antigen binding, followed by the strong interaction of the R_8 moieties with the cell. The low cell-bound radioactivity of [^{125}I]SIB-NuB2$_I$ in the presence of excess NuB2 suggested slower interaction kinetics of R_8 moieties with the cell, following the specific binding. However, when the dissociation rates from the cells were compared, not only [^{125}I]SIB-NuB2$_{III}$ but also [^{125}I]SIB-NuB2$_I$ exhibited much longer residence times in the CD20 positive tumor cells than [^{125}I]SIB-NuB2 (Figure 2C). The confocal microscopy confirmed that both NuB2$_I$ and NuB2$_{III}$ were present on the cell membrane (Figure 2A). These studies supported the hypothesis that the conjugation of anchoring molecules that possess strong interaction with cell surface molecules or cell membrane prolonged the retention of radiolabeled antibodies on tumor cells by fixing the antigen-bound antibodies on target cells, although the binding kinetics of anchoring molecules with the cell was affected by their density. This also suggested that further improvement of spatial location of the R_8 molecule may increase the binding kinetics.

Despite favorable anchoring ability, the heavy conjugation of R_8 affected biodistribution profiles of the parental antibody. As shown in Table 1, [^{125}I]SIB-NuB2$_{III}$ displayed faster clearance from the blood and higher accumulation in the liver in normal mice, as also observed in prior studies (*30*). On the other hand, both [^{125}I]SIB-NuB2 and [^{125}I]SIB-NuB2$_I$ displayed similar biodistribution (Table 1). These results reinforced the importance of the number of R_8 molecules attached per molecule of an antibody to retain its in vivo behavior (*10, 11*) and showed that the present conjugation of up to 2 R_8 molecules per molecule of NuB2 did not induce any significant changes in biodistribution. Recently, we have observed that the biodistribution of PAMAM dendrimers is predominantly determined by their net molecular charge as measured by both zeta potential and pI values (*31*). The present study also suggests that the determination of net molecular charge of AR-CPP-modified antibodies may be useful to predict their pharmacokinetics.

The biodistribution studies in tumor-bearing SCID mice were investigated with [^{125}I]SIB-NuB2 and [^{131}I]SIB-NuB2$_I$ since they exhibited similar pharmacokinetics in normal mice. To minimize individual differences, the biodistribution studies were conducted after injection of a mixed solution of [^{131}I]SIB-NuB2$_I$ and [^{125}I]SIB-NuB2. As shown in Table 2, the role played by R_8 conjugation on tumor accumulation was clearly demonstrated in the biodistribution studies, where [^{131}I]SIB-NuB2$_I$ exhibited significantly higher radioactivity levels in the xenograft than those of simultaneously administrated [^{125}I]SIB-NuB2 with no significant increase being observed in the radioactivity levels of blood, liver, and other tissues between the two. When considering the in vitro studies, these results would be attributable to the delayed dissociation rates of [^{131}I]SIB-NuB2$_I$ from the target cells in vivo.

In conclusion, the findings in this study indicated that the conjugation of anchoring molecules to an antibody that possesses a strong interaction with cell surface molecules or cell membrane enhanced accumulation in target tissues by fixing antigen-bound antibodies on target cells. This study also showed that conjugation of up to 2 molecules of R_8 per molecule of NuB2 satisfied both target-specific binding of antibodies and strong cell binding property of R_8. Further optimization of the conjugation chemistry would be required to provide uniform conjugates with appropriate linkage structure between R_8 and an antibody. These findings strongly suggested the application of AR-CPP to enhance specific accumulation of antibodies in target for more effective RIT.

ACKNOWLEDGMENT

The authors appreciated to Immuno-Biological Laboratories Co, Ltd., for supplying the relevant and irrelevant antibodies. Y. Azuma is grateful for the JSPS Research Fellowship for Young Scientists. This work was supported in part by a Grant-in-Aid for Scientific Research (B), for Exploratory Research,

for Development of Systems and Technology for Advanced Measurement and Analysis, and by Special Funds for Education and Research (Development of SPECT Probes for Pharmaceutical Innovation) from the Ministry of Education, Culture, Sports, Science, and Technology, Japan. This work was dedicated to our distinguished colleague, the late Mr. Yuichiro Taira.

LITERATURE CITED

(1) Fisher, R. I., Kaminski, M. S., Wahl, R. L., Knox, S. J., Zelenetz, A. D., Vose, J. M., Leonard, J. P., Kroll, S., Goldsmith, S. J., and Coleman, M. (2005) Tositumomab and iodine-131 tositumomab produces durable complete remissions in a subset of heavily pretreated patients with low-grade and transformed non-Hodgkin's lymphomas. *J. Clin. Oncol. 23*, 7565–7573.

(2) Vose, J. M. (2004) Bexxar: novel radioimmunotherapy for the treatment of low-grade and transformed low-grade non-Hodgkin's lymphoma. *Oncologist 9*, 160–172.

(3) Gordon, L. I., Molina, A., Witzig, T., Emmanouilides, C., Raubtischek, A., Darif, M., Schilder, R. J., Wiseman, G., and White, C. A. (2004) Durable responses after ibritumomab tiuxetan radioimmunotherapy for $CD20^+$ B-cell lymphoma: long-term follow-up of a phase 1/2 study. *Blood 103*, 4429–4431.

(4) Witzig, T. E., White, C. A., Wiseman, G. A., Gordon, L. I., Emmanouilides, C., Raubitschek, A., Janakiraman, N., Gutheil, J., Schilder, R. J., Spies, S., Silverman, D. H., Parker, E., and Grillo-Lopez, A. J. (1999) Phase I/II trial of IDEC-Y2B8 radioimmunotherapy for treatment of relapsed or refractory CD20(+) B-cell non-Hodgkin's lymphoma. *J. Clin. Oncol. 17*, 3793–803.

(5) von Mehren, M., Adams, G. P., and Weiner, L. M. (2003) Monoclonal antibody therapy for cancer. *Annu. Rev. Med. 54*, 343–369.

(6) Goldenberg, D. M. (2001) The role of radiolabeled antibodies in the treatment of non-Hodgkin's lymphoma: the coming of age of radioimmunotherapy. *Crit. Rev. Oncol. Hematol. 39*, 195–201.

(7) Boswell, C. A., and Brechbiel, M. W. (2007) Development of radioimmunotherapeutic and diagnostic antibodies: an inside-out view. *Nucl. Med. Biol. 34*, 757–778.

(8) Jain, M., Venkatraman, G., and Batra, S. K. (2007) Optimization of radioimmunotherapy of solid tumors: biological impediments and their modulation. *Clin. Cancer Res. 13*, 1374–1382.

(9) Tempero, M., Leichner, P., Baranowska-Kortylewicz, J., Harrison, K., Augustine, S., Schlom, J., Anderson, J., Wisecarver, J., and Colcher, D. (2000) High-dose therapy with ^{90}Yttrium-labeled monoclonal antibody CC49: a phase I trial. *Clin. Cancer Res. 6*, 3095–3102.

(10) Anderson, D. C., Nichols, E., Manger, R., Woodle, D., Barry, M., and Fritzberg, A. R. (1993) Tumor cell retention of antibody Fab fragments is enhanced by an attached HIV TAT protein-derived peptide. *Biochem. Biophys. Res. Commun. 194*, 876–884.

(11) Niesner, U., Halin, C., Lozzi, L., Günthert, M., Neri, P., Wunderli-Allenspach, H., Zardi, L., and Neri, D. (2002) Quantitation of the tumor-targeting properties of antibody fragments conjugated to cell-permeating HIV-1 TAT peptides. *Bioconjugate Chem 13*, 729–736.

(12) Batra, S. K., Jain, M., Wittel, U. A., Chauhan, S. C., and Colcher, D. (2002) Pharmacokinetics and biodistribution of genetically engineered antibodies. *Curr. Opin. Biotechnol. 13*, 603–608.

(13) Goel, A., Colcher, D., Baranowska-Kortylewicz, J., Augustine, S., Booth, B. J., Pavlinkova, G., and Batra, S. K. (2000) Genetically engineered tetravalent single-chain Fv of the pancarcinoma monoclonal antibody CC49: improved biodistribution and potential for therapeutic application. *Cancer Res. 60*, 6964–6971.

(14) Boerman, O. C., van Schaijk, F. G., Oyen, W. J., and Corstens, F. H. (2003) Pretargeted radioimmunotherapy of cancer: progress step by step. *J. Nucl. Med. 44*, 400–411.

(15) Rothbard, J. B., Jessop, T. C., Lewis, R. S., Murray, B. A., and Wender, P. A. (2004) Role of membrane potential and hydrogen bonding in the mechanism of translocation of guanidinium-rich peptides into cells. *J. Am. Chem. Soc. 126*, 9506–9507.

(16) Sakai, N., Takeuchi, T., Futaki, S., and Matile, S. (2005) Direct observation of anion-mediated translocation of fluorescent oligoarginine carriers into and across bulk liquid and anionic bilayer membranes. *ChemBioChem 6*, 114–122.

(17) Nakase, I., Takeuchi, T., Tanaka, G., and Futaki, S. (2008) Methodological and cellular aspects that govern the internalization mechanisms of arginine-rich cell-penetrating peptides. *Adv. Drug Delivery Rev. 60*, 598–607.

(18) Goncalves, E., Kitas, E., and Seelig, J. (2005) Binding of oligoarginine to membrane lipids and heparan sulfate: structural and thermodynamic characterization of a cell-penetrating peptide. *Biochemistry 44*, 2692–2702.

(19) Kaplan, I. M., Wadia, J. S., and Dowdy, S. F. (2005) Cationic TAT peptide transduction domain enters cells by macropinocytosis. *J. Controlled Release 102*, 247–253.

(20) Nakase, I., Niwa, M., Takeuchi, T., Sonomura, K., Kawabata, N., Koike, Y., Takehashi, M., Tanaka, S., Ueda, K., Simpson, J. C., Jones, A. T., Sugiura, Y., and Futaki, S. (2004) Cellular uptake of arginine-rich peptides: roles for macropinocytosis and actin rearrangement. *Mol. Ther. 10*, 1011–1022.

(21) Richard, J. P., Melikov, K., Vives, E., Ramos, C., Verbeure, B., Gait, M. J., Chernomordik, L. V., and Lebleu, B. (2003) Cell-penetrating peptides. A reevaluation of the mechanism of cellular uptake. *J. Biol. Chem. 278*, 585–590.

(22) Arano, Y., Wakisaka, K., Ohmono, Y., Uezono, T., Akizawa, H., Nakayama, M., Sakahara, H., Tanaka, C., Konishi, J., and Yokoyama, A. (1996) Assessment of radiochemical design of antibodies using an ester bond as the metabolizable linkage: evaluation of maleimidoethyl 3-(tri-n-butylstannyl)hippurate as a radioiodination reagent of antibodies for diagnostic and therapeutic applications. *Bioconjugate Chem. 7*, 628–637.

(23) Percy, M. E., Baumal, R., Dorrington, K. J., and Percy, J. R. (1976) Covalent assembly of mouse immunoglobulin G subclasses in vitro: application of a theoretical model for interchain disulfide bond formation. *Can. J. Biochem. 54*, 675–87.

(24) Grassetti, D. R., and Murray, J. F., Jr. (1967) Determination of sulfhydryl groups with 2,2′- or 4,4′-dithiodipyridine. *Arch. Biochem. Biophys. 119*, 41–49.

(25) Zalutsky, M. R., and Narula, A. S. (1987) A method for the radiohalogenation of proteins resulting in decreased thyroid uptake of radioiodine. *Int. J. Rad. Appl. Instrum. A 38*, 1051–1055.

(26) Koizumi, M., Endo, K., Kunimatsu, M., Sakahara, H., Nakashima, T., Kawamura, Y., Watanabe, Y., Saga, T., Konishi, J., and Yamamuro, T. (1988) ^{67}Ga-labeled antibodies for immunoscintigraphy and evaluation of tumor targeting of drug-antibody conjugates in mice. *Cancer Res. 48*, 1189–1194.

(27) Samnick, S., Schaefer, A., Siebert, S., Richter, S., Vollmar, B., and Kirsch, C. M. (2001) Preparation and investigation of tumor affinity, uptake kinetic and transport mechanism of iodine-123-labelled amino acid derivatives in human pancreatic carcinoma and glioblastoma cells. *Nucl. Med. Biol. 28*, 13–23.

(28) Foulon, C. F., Reist, C. J., Bigner, D. D., and Zalutsky, M. R. (2000) Radioiodination via D-amino acid peptide enhances cellular retention and tumor xenograft targeting of an internalizing anti-epidermal growth factor receptor variant III monoclonal antibody. *Cancer Res. 60*, 4453–4460.

(29) Meares, C. F., and Goodwin, D. A. (1984) Linking radiometals to proteins with bifunctional chelating agents. *J. Protein Chem. 3*, 215–228.

(30) Kameyama, S., Horie, M., Kikuchi, T., Omura, T., Takeuchi, T., Nakase, I., Sugiura, Y., and Futaki, S. (2006) Effects of cell-permeating peptide binding on the distribution of ^{125}I-labeled Fab fragment in rats. *Bioconjugate Chem. 17*, 597–602.

(31) Uehara, T., Ishii, D., Uemura, T., Suzuki, H., Kanei, T., Takagi, K., Takama, M., Murakami, M., Akizawa, H., and Arano, Y. (2010) gamma-Glutamyl PAMAM dendrimer as versatile precursor for dendrimer-based targeting devices. *Bioconjugate Chem. 21*, 175–181.

BC100259Q